Direct Contact Membrane Distillation-Based Desalination: Novel Membranes, Devices, Larger-Scale Studies, and a Model

Liming Song, Baoan Li,[†] Kamalesh K. Sirkar,* and Jack L. Gilron[‡]

Otto H. York Department of Chemical Engineering, Center for Membrane Technologies, New Jersey Institute of Technology, Newark, New Jersey 07032

We report here direct contact membrane distillation results from modules having 0.28 m^2 of membrane surface area employing porous hydrophobic polypropylene hollow fibers of internal diameter (330 μm) and wall thickness (150 μm) with a porous fluorosilicone coating on the outside surface. The brine salt concentration and temperature and the distillate temperature and velocity were varied. Water vapor fluxes approach values obtained earlier in much smaller modules. As the brine temperature was increased from 40 to 92 °C, water vapor flux increased almost exponentially. Increasing the distillate temperature to 60 from 32 °C yielded reasonable fluxes. Salt concentration increases to 10% led to a small flux reduction. An extended 5-day run did not show any pore wetting. A model using the mass transfer coefficient k_m as an adjustable parameter predicted the brine temperature drop, distillate temperature rise, and water vapor flux well for the large module and the smaller module of 119-cm^2 surface area.

Introduction

The desalination of brine is commercially implemented by reverse osmosis (RO) and thermal processes like multistage flash (MSF) distillation. Although such conventional processes are widely used, there is a need for novel desalination techniques which are cheaper than both RO and MSF processes or have other distinct advantages. Membrane distillation (MD) is potentially one such process. In one variety of the MD process, namely, direct contact membrane distillation (DCMD), a hot nonvolatile solute-containing aqueous solution, e.g., hot brine, is passed on one side of a porous hydrophobic membrane as a colder aqueous distillate stream flows on the other side. Diffusion of water vapor evaporated from the hot brine at the brine−membrane interface takes place through the gas-filled hydrophobic membrane pores; the water vapor is condensed in the cold distillate on the other side of the membrane, the distillate−membrane interface (Figure 1a). In another variety of MD, namely, vacuum membrane distillation (VMD), there is no cold distillate stream on the other side of the membrane; instead, a vacuum is maintained. The water vapor is condensed and recovered as the distillate in a separate condenser.

Of these two MD processes, DCMD is quite attractive since it eliminates the need for a separate condenser. It operates at around atmospheric pressure and can treat brines of various salt concentrations since it is not subject to the osmotic pressure-driven limitations of RO. Since the earliest reports of DCMD by Findley[1] and Gore,[2] many studies have been made and reviews have been published.[3−12] These studies have identified the need to reduce temperature polarization on the hot brine side (Figure 1b): the value of T_{fm} should be as close to the bulk brine temperature T_f as possible so that water vapor pressure at the hot brine−pore interface is as high as possible. This ensures a high partial pressure difference of water vapor across the gas-filled membrane pore. However, the conductive heat loss through the solid polymeric wall of the membrane as well as the gas−vapor pathway in the membrane pore should also be reduced drastically to ensure that the sensible heat of the hot brine is primarily utilized to vaporize water at the brine−membrane surface. These conditions dictate thicker wall membranes having as high a porosity as possible: conductive heat flux is reduced; the water vapor transport coefficient through the membrane may be potentially increased. In addition, the distillate temperature should remain low to maintain a high water vapor pressure difference between the two sides of the membrane pore.

Most studies mentioned earlier used hydrophobic membranes of polypropylene, polytetrafluroethylene, polyvinylidene fluoride, etc. having high porosities, 0.3−0.8, and larger pore sizes, 0.1 − 0.6 μm. Such membranes are not supposed to get wetted by hot brine flowing at atmospheric pressure as long as the pressure difference between the two sides does not exceed the breakthrough pressure (Δp_{br}).[4,5] Often, however, the water vapor flux has been observed to suffer from a decay with time. Investigators have surmised that this is due to pore wetting as well as pore fouling, scaling, etc.[4,6,13−16]. Preventing/controlling such wetting/fouling via suitable membrane design is of considerable interest.

To address these and other issues, we carried out preliminary DCMD investigations in a very small scale using hollow fiber membranes and modules having a number of novel features;[17] in addition, VMD studies were also carried out.[18] First, a crossflow module design was implemented in which the hot brine flowed perpendicular to the axis of the hollow fibers to ensure a high heat transfer coefficient (Figure 1c) at a low Reynolds number. It is known that crossflow can enhance mass transport coefficients by a few times at quite low Reynolds numbers compared to parallel flow.[19] Second, an ultrathin highly porous layer of silicone fluoropolymer was deposited on the outside surface of hydrophobic porous hollow fibers of polypropylene (PP) by plasma polymerization (Figure 1d). The porous PP hollow fibers selected had a large pore size >0.2 μm. The reason for applying the coating was not to reduce this PP substrate pore size but to provide an additional porous highly hydrophobic layer (having a higher hydrophobicity than that of PP). Further if this layer has larger pores, it will act as a buffer layer. Should there be accidental wetting via wetting

* To whom correspondence should be addressed. Tel.: 1-973-596-8447. Fax: 1-973-642-4854. E-mail: Sirkar@adm.njit.edu.

[†] Current address: Chemical Engineering Research Center, Tianjin University, China.

[‡] On leave from Ben-Gurion University, Beer-Sheva, Israel.

10.1021/ie0609968 CCC: $37.00
Published on Web 02/27/2007

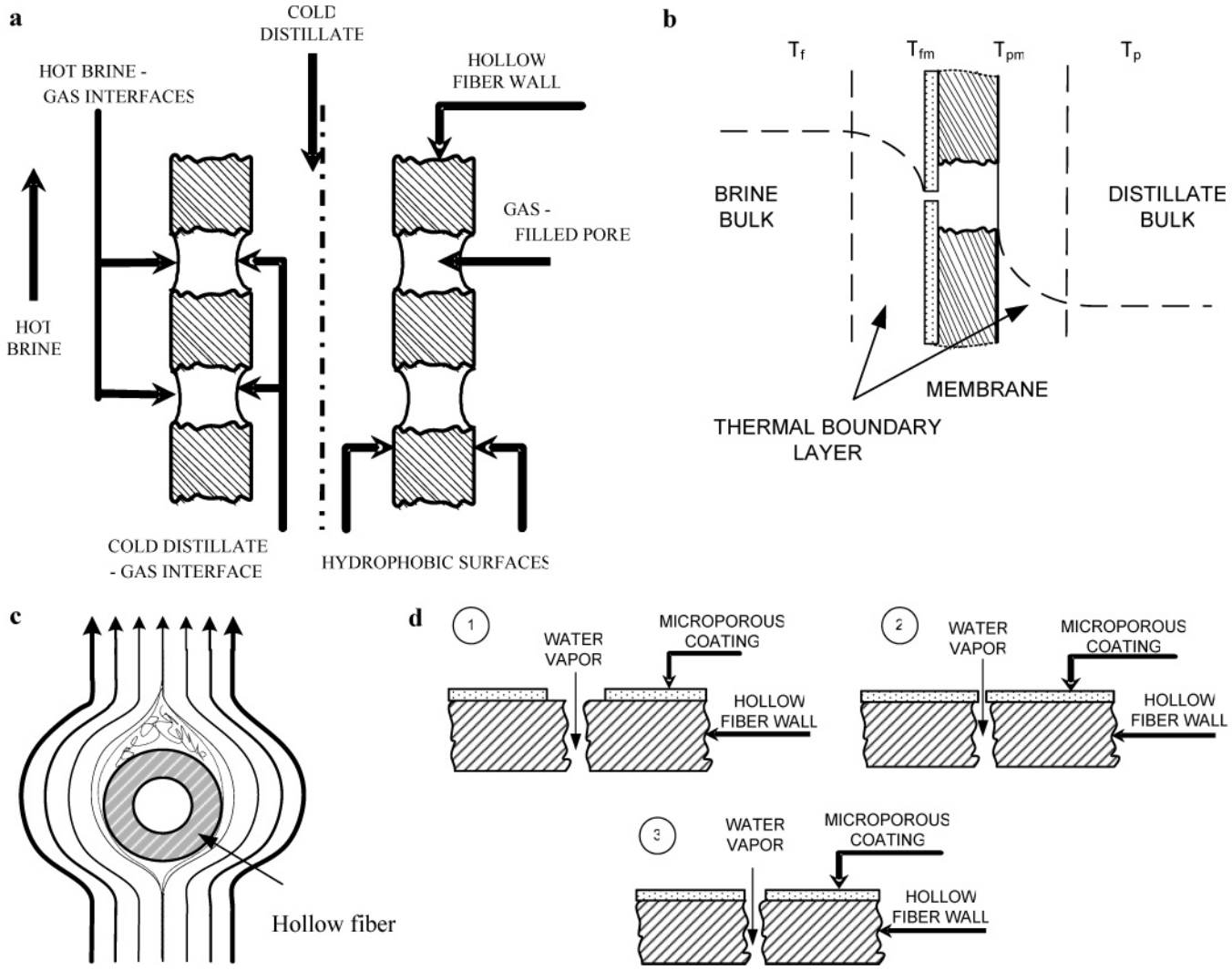

Figure 1. (a) Conventional direct contact membrane distillation. (b) Temperature profile across the DCMD membrane. (c) Crossflow over hollow fiber o.d. (d) Water vapor flowing through porous hydrophobic coating on the surface of porous hollow fiber membrane.

precursors/deposits, the buffer layer will get wetted but not the substrate PP layer. To be noted is that the critical surface tension of this coating was much less than that of a PP surface.

These were additional features in the small modules/devices studied in DCMD.[17] The hollow fibers selected had a wall thickness of 150 μm considerably larger than that in conventional porous hydrophobic hollow fibers; this reduced the conductive heat loss substantially. Further, the fiber walls were highly porous, the porosity being around 0.65. The high porosity reduced the conductive heat flux while reducing the resistance for water vapor diffusion through the pores. In addition, the hollow fibers employed had a much larger internal diameter of 330 μm to reduce the distillate pressure drop. It is highly important to maintain a large distillate flow rate through the fiber bore so that the distillate temperature rise can be controlled with a limited expenditure of pressure energy. The distillate temperature rise should be controlled to maintain as high a vapor pressure difference between the hot brine and the colder distillate; the latter is essential to achieving a high water vapor flux.

The synergistic combination of these novel features yielded very high water vapor fluxes in DCMD of as much as 60−79 kg/(m^2 h) from hot brine feeds of 85−90 °C in a small module having a hollow fiber membrane surface area of 119 cm^2 (based on the fiber's inside diameter).[17] This is more than a few times of what is achieved in conventional seawater RO. Since hollow fiber membrane devices are relatively simple, can pack considerable surface area per unit volume, and may be scaled up without great difficulty, these high flux results[17] are of considerable importance. A number of issues naturally arise. Can one achieve such high fluxes in larger membrane modules? Is there any scale-dependence in this behavior? Can one model the observed behavior vis-à-vis the water vapor flux? How does fouling, etc., affect the flux over an extended period of time? Li and Sirkar[17] studied desalination in their small DCMD module using a hot brine concentration of 1% NaCl. What is the effect of increasing brine concentration on the observed water vapor flux? Could one make progress toward zero liquid discharge (ZLD) by going to high brine concentrations?

We have addressed these issues in the present work. We have scaled up the hollow fiber membrane device by increasing the membrane surface area from 119 to 2864 cm^2 (0.28 m^2) in a single module. We have investigated the water flux behavior as the salt concentration in brine was increased from 1% to 3%, 6%, and 10%. We have further varied the distillate inlet temperature to observe how the water vapor flux is reduced with an increase in distillate inlet temperature. We have also developed a model to predict the hot brine temperature drop, distillate temperature rise, and the water vapor flux as the inlet brine temperature and the interstitial velocity of the hot brine is varied in crossflow across the fibers. This model has also been used to predict the observed behavior of flux dependence

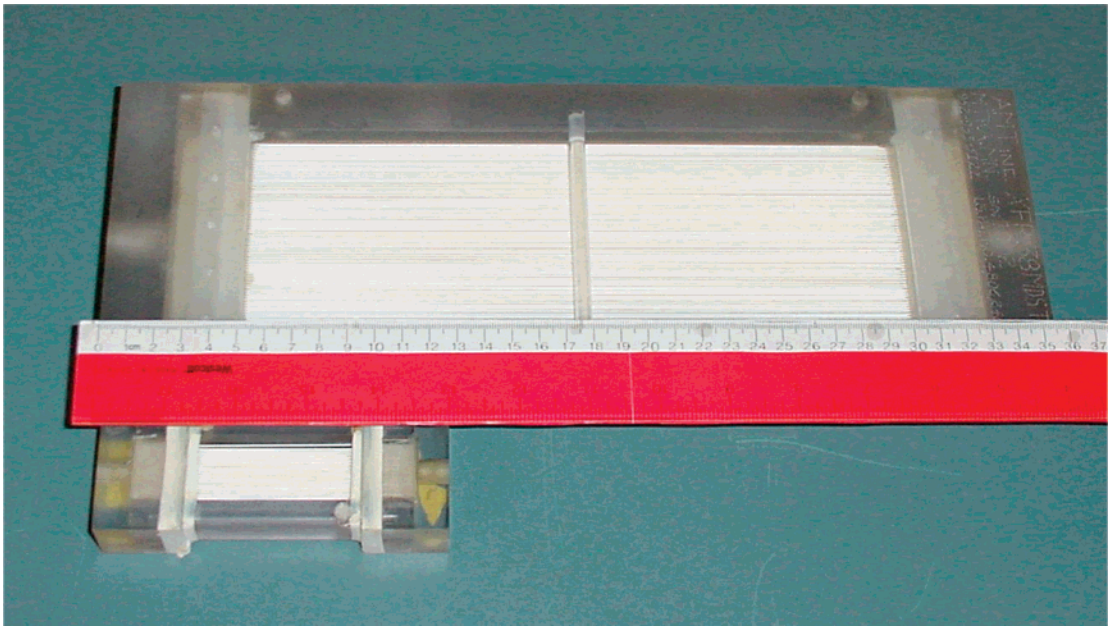

Figure 2. Photo of small size membrane module and larger size module used in this research with a scale in between.

on the interstitial velocity in the much smaller modules of the earlier study.[17] We have also modeled how the water vapor flux and the various temperatures of interest change with fiber length as the brine crosses one fiber layer into another. The development of this model was considerably aided by our recent study[18] of vacuum membrane distillation (VMD) using the same smaller membrane modules studied in the DCMD process.[17]

Modeling Considerations. Figure 2 shows the photos of the DCMD modules without the cover plates at two scales. Details of these modules' dimensions are provided in the experimental section. Hot brine flows perpendicular to the fibers in the picture frame as the cold distillate is introduced to the bore of the fibers at one end and exits as the heated distillate at the other end of the fibers. An approximate schematic of the staggered fiber arrangement vis-à-vis the hot brine flow is shown in Figure 3a for the larger module S/N 1004 (having 16 consecutive layers of fibers compared with ten layers in the much smaller module[17] MXFR#3). If we consider now any fiber layer (e.g., jth layer, $j = 1, 2, ..., m$), on the distillate side, the distillate volume flow rate coming in is $V_{p0,j}$ at a temperature $T_{p0,j}$; the corresponding values at the exit of the fiber length L are $V_{p1,j}$ and $T_{p1,j}$ (Figure 3b). However, we have a more complex situation on the brine side. The local hot brine velocity and temperature depend on the location along the fiber length since the water evaporation rate depends on the location. Therefore, we will now define a few variables used in our model to describe the local brine flow conditions (velocity and temperature). The length coordinate along the distillate flow direction is x. Define now $V'_{f0,j}(x)$ and $T_{f0,j}(x)$ and $V'_{f1,j}(x)$ and $T_{f1,j}(x)$ as the local brine inlet volumetric flow rate per unit fiber length and temperature and the local brine outlet volumetric flow rate per unit fiber length and temperature, respectively, for the fibers in the jth layer. Over a small length Δx of the fibers in the jth layer, the local values of $V_{p1,j}$, $T_{p1,j}$, namely, $V_{p1,j}(x)$ and $T_{p1,j}(x)$ change to $V_{p1,j}(x + \Delta x)$ and $T_{p1,j}(x + \Delta x)$ (Figure 3c); correspondingly, $V'_{f0,j}(x)$ and $T_{f0,j}(x)$ are changed beyond the jth layer to $V'_{f1,j}(x)$ and $T_{f1,j}(x)$. The inlet and outlet brine volumetric flow rates for the jth layer $V_{b0,j}$ and $V_{b1,j}$, can be calculated by integrating $V'_{f0,j}(x)$ and $V'_{f1,j}(x)$ over the fiber length from $x = 0$ to $x = L$, respectively (Figure 3b). The inlet and outlet brine temperatures $T_{b0,j}$ and

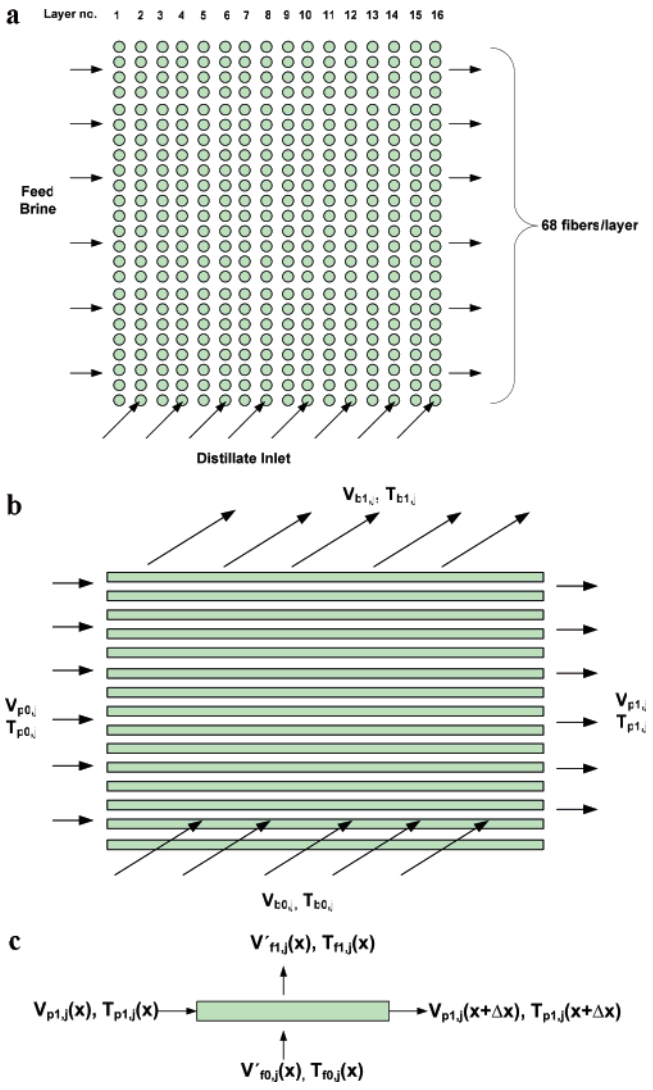

Figure 3. (a) Arrangement of fibers in DCMD module. (b) Schematic of the jth layer in the DCMD module. (c) Mass and energy balance for the length of Δx in the distillate flow direction.

$T_{b1,j}$ are the cup-mixing values of $T_{f0,j}(x)$ and $T_{f1,j}(x)$ over the fiber length based on an energy balance. For the first fiber layer ($j = 1$), $V_{b0,j}$ and $T_{b0,j}$ are known from the brine feed conditions. Correspondingly, for $j = 1$, $V'_{f0,j}(x)$ ($= V_{b0,j}/L$) and $T_{f0,j}(x)$ ($= T_{b0,j}$) are constant from $x = 0$ to $x = L$. At the distillate entrance location ($x = 0$), the water vapor flux is highest, and therefore, the temperature drop in the hot brine, e.g., $(T_{f0,j}(x) - T_{f1,j}(x))$, will be highest and so will be the hot brine velocity reduction (which however is of a very small magnitude). At any location x, the bulk brine temperature T_f drops to T_{fm} at the membrane surface (Figure 1b); the corresponding quantities for numerical calculations are $T_{f0,j}(x)$ and $T_{fm,j}(x)$. On the distillate side, the temperature T_{pm} at the membrane surface drops to the bulk distillate temperature T_p with corresponding notational changes to $T_{pm,j}(x)$ and $T_{p1,j}(x)$.

As we now go to the next layer of fibers (the $(j + 1)$th layer), we make a basic assumption, namely, there is no lateral mixing in the x-direction of the hot brine between two consecutive fiber layers. Therefore, the hot brine velocity and temperature being imposed on the $(j + 1)$th layer of fibers depends on the fiber length coordinate x and are obtained as output from the calculations for the previous layer of fibers (jth layer). This process is continued until the last layer of fibers in a given module. Consequently, our computational scheme proceeds from fiber layer to layer for a given hot brine input at the first fiber layer and a constant flow rate and temperature input into all fibers in all layers on the distillate side. Ideally, there may be minor variations in distillate-side flow rate with the layer number since as the brine temperature decreases with increasing layer number, the temperature decreases in brine lead to a lower temperature rise in the distillate and, therefore, an increasing viscosity and, consequently, a lower flow rate since the pressures at the fiber inlet and outlet on the distillate side are essentially the same regardless of the layer number. For given distillate feed conditions (i.e., inlet volumetric flow rate V_{d0} and temperature T_{d0}), for each fiber layer $V_{p0,j}$ ($= V_{d0}/m$, where m is the number of fiber layers) and $T_{p0,j}$ ($= T_{d0}$) are constant. Correspondingly, the distillate outlet volumetric flow rate V_{d1} is the sum of $V_{p1,j}$ for all fiber layers, and the distillate outlet temperature T_{d1} is the flow weighted average of $T_{p1,j}$ for all fiber layers based on energy balance.

We will now write the local equations for heat transfer in brine for the jth fiber layer containing n fibers of internal diameter d_i and outer diameter d_o over a length dx of the fiber at location x. The expression below is the heat transfer rate per unit length.

Shell-Side Hot Brine: Heat Transfer.

$$\left.\frac{dQ(x)}{dx}\right|_j = h_f A_{rf} \alpha (T_{f0,j}(x) - T_{fm,j}(x)) \tag{1}$$

where

$$A_{rf} = \left(\frac{d_o}{d_i}\right), \quad \alpha = n\pi d_i \tag{2}$$

In our VMD paper,[18] we have observed that Žukauskas' equation[20] (3a/3b)

$$Nu_f = \frac{h_f d_o}{k_o} = 1.04 Re_o^{0.4} Pr_o^{0.36} \left(\frac{Pr_o}{Pr_w}\right)^{0.25} F_c \quad (Re_o < 40) \tag{3a}$$

$$Nu_f = \frac{h_f d_o}{k_o} = 0.71 Re_o^{0.5} Pr_o^{0.36} \left(\frac{Pr_o}{Pr_w}\right)^{0.25} F_c \quad (Re_o > 40) \tag{3b}$$

appears to describe the observed variation of water vapor flux with brine flow velocity quite well. Therefore, we use this equation to calculate the heat transfer coefficient h_f on the brine side for given values of the Reynolds number Re_o and Pr_o:

$$Re_o = \frac{d_o u_o \rho_o}{\mu_o}; \quad Pr_o = \frac{C_{po}\mu_o}{k_o}; \quad Pr_w = \frac{C_{pw}\mu_w}{k_w} \tag{4}$$

Tube-Side Distillate: Heat Transfer. The equation corresponding to eq 1 for the tube-side distillate is

$$\frac{dQ(x)}{dx}\Big|_j = h_p A_{rp} \alpha (T_{pm,j}(x) - T_{p1,j}(x)) \tag{5}$$

$$A_{rp} = \frac{d_i}{d_i} (= 1) \tag{6}$$

The heat transfer coefficient h_p in the permeate (i.e., distillate) side may be described in a number of ways. One of them is based on the Sieder−Tate equation:[21]

$$Nu_p = \frac{h_p d_i}{k_i} = 1.86 \left(\frac{d_i}{L}\right)^{0.33} (Re_i Pr_i)^{0.33} \left(\frac{\mu_i}{\mu_{wi}}\right)^{0.14} \tag{7a}$$

$$Re_i = \frac{d_i u_i \rho_i}{\mu_i}; \quad Pr_i = \frac{C_{pi}\mu_i}{k_i} \tag{7b}$$

Heat Transfer across the Porous Membrane. Heat is transferred from the hot brine−membrane interface to the distillate−membrane interface in two ways. Water vapor flux convection creates an enthalpy flux, and there is conductive flux through the solid matrix as well as the porous gas space (porosity of the membrane, ϵ_m):[22]

$$\frac{dQ(x)}{dx}\Big|_j = h_m A_{rln} \alpha (T_{fm,j}(x) - T_{pm,j}(x)) + N_{v,j}(x) \alpha (\Delta H_v (T_{pm,j}(x)) + C_{pm,j} T_{pm,j}(x)) \tag{8}$$

$$h_m = \epsilon_m h_{mg} + (1 - \epsilon_m) h_{ms} \tag{9}$$

The second term on the right-hand side of eq 8 involves expressing the enthalpy of the water vapor as it is added to the distillate at the distillate−membrane interface; here, the basis of enthalpy calculations is liquid water at a temperature of 0 °C. The quantity $N_{v,j}(x)$ is the water vapor mass flux in the jth fiber layer at any x. The area ratios relevant are

$$A_{rln} = \frac{d_{lm}}{d_i}; \quad d_{lm} = \frac{d_o - d_i}{\ln\left(\frac{d_o}{d_i}\right)}; \quad A_{rp} = 1 = \frac{d_i}{d_i} \tag{10}$$

The heat transfer coefficient for the solid polymeric matrix h_{ms} is defined by

$$h_{ms} = \frac{2k_{ms}}{(d_o - d_i)} \tag{11a}$$

where k_{ms} is the thermal conductivity of the matrix material. The corresponding quantity for the gas phase is

$$h_{mg} = \frac{2k_{mg}}{(d_o - d_i)} \tag{11b}$$

Both of these quantities are defined with respect to the total surface area of the fibers: their individual area effects are taken into account via ϵ_m in eq 9.

Heat Transferred by the Hot Brine. The heat lost by the hot brine per unit fiber length from the jth fiber layer at any location x is

$$\frac{dQ(x)}{dx}|_j = \rho_{f0,j}(x)V'_{f0,j}(x)C_{pf0,j}(x)T_{f0,j}(x) - \rho_{f1,j}(x)V'_{f1,j}(x)C_{pf1,j}(x)T_{f1,j}(x) \tag{12}$$

Here $V'_{f0,j}(x)$ and $V'_{f1,j}(x)$ are defined above as the local brine inlet and outlet volumetric brine flow rates per unit fiber length for the jth layer. For the first fiber layer, $V'_{f0,1}(x)$ (= $V_{b0,1}/L$) and $T_{f0,1}(x)$ (= $T_{b0,1}$) are constant for a given brine feed flow rate $V_{b0,1}$ and feed temperature $T_{b0,1}$. The rate of thermal energy gain by the distillate flow from the fiber entrance ($x = 0$) to axial location x is obtained by integrating eq 5 along x and equating it to the rate of enthalpy gain by the distillate:

$$Q(x)|_j = \int_0^x dQ(x)|_j = \int_0^x h_p A_{rp}\alpha(T_{pm,j}(x) - T_{p1,j}(x))\,dx \tag{13a}$$

$$Q(x)|_j = \rho_{p1,j}(x)V_{p1,j}(x)C_{p1,j}(x)T_{p1,j}(x) - \rho_{p0,j}V_{p0,j}C_{p0,j}T_{p0,j} \tag{13b}$$

Water Vapor Flux in a Fiber Layer at Any x. As is generally practiced in the literature, the water vapor mass flux is to be described using a membrane mass transfer coefficient k_m (here $N_{v,j}(x)$ is defined based on i.d.)

$$N_{v,j}(x) = k_m A_{rln}(p_{fm,j}(x) - p_{pm,j}(x)) \tag{14}$$

Integration of this expression along the length of the fiber for n fibers in a given layer for the jth layer yields

$$\int_0^L N_{v,j}(x)\alpha\,dx = \rho_{b0,j}V_{b0,j} - \rho_{b1,j}V_{b1,j} \tag{15}$$

A corresponding result on the permeate side from $x = 0$ to x leads to

$$\int_0^x N_{v,j}(x)\alpha\,dx = \rho_{p1,j}(x)V_{p1,j}(x) - \rho_{p0,j}V_{p0,j} \tag{16}$$

The driving partial pressure of water at location x in the hot brine in the jth fiber layer, namely, $p_{fm,j}(x)$ may be estimated from the Antoine equation[23] by assuming vapor−liquid equilibrium and an activity coefficient of water equal to 1:

$$p_{fm,j}(x) \cong p^0_{fm,j}(x) = 10^3 \exp\left(16.260 - \frac{3799.89}{T_{fm,j}(x) + 273.15 - 46.8}\right) \tag{17a}$$

The corresponding partial pressure of water vapor on the permeate side is

$$p_{pm,j}(x) \cong p^0_{pm,j}(x) = 10^3 \exp\left(16.260 - \frac{3799.89}{T_{pm,j}(x) + 273.15 - 46.8}\right) \tag{17b}$$

To be exact, these expressions are actually the vapor pressure of water $p^0_{fm,j}(x)$ and $p^0_{pm,j}(x)$ on the feed interface and the distillate interface, respectively. The actual water vapor partial pressures are related to these two values via

$$p_{fm,j}(x) = x_{fm}\gamma_{fm}p^0_{fm,j}(x); \quad p_{pm,j}(x) = x_{pm}\gamma_{pm}p^0_{pm,j}(x) \tag{18a}$$

where γ_{fm} and γ_{pm} are the activity coefficients of water at those locations and x_{fm} and x_{pm} are the corresponding water mole fractions. The activity coefficient of water γ_{water} has been related to the salt mole fraction x_{NaCl} via[6]

$$\gamma_{water} = 1 - 0.5x_{NaCl} - 10x_{NaCl}^2 \tag{18b}$$

In this analysis, the dependent variables for the jth layer that are unknown are as follows: $Q(x)|_j$, $T_{fm,j}(x)$, $T_{pm,j}(x)$, $T_{p1,j}(x)$, $p_{fm,j}(x)$, $p_{pm,j}(x)$, $N_{v,j}(x)$, $V'_{f1,j}(x)$, $T_{f1,j}(x)$, $V_{p1,j}(x)$. Of these, $p_{fm,j}(x)$, $p_{pm}(x)$, $T_{f1,j}(x)$, $Q(x)|_j$, and $V'_{f1,j}(x)$ depend on the other five primary variables. We have correspondingly the following equations:

$$Q(x)|_j = \int_0^x h_p A_{rp}\alpha(T_{pm,j}(x) - T_{p,j}(x))\,dx = \rho_{p1,j}(x)V_{p1,j}(x)C_{p1,j}(x)T_{p1,j}(x) - \rho_{0,j}V_{p0,j}C_{p0,j}T_{p0,j} \tag{13a,b}$$

$$N_{v,j}(x) = k_m A_{rln}(p_{fm,j}(x) - p_{pm,j}(x)) \tag{14}$$

$$\int_0^x N_{v,j}(x)\alpha\,dx = \rho_{p1,j}(x)V_{p1,j}(x) - \rho_{p0,j}V_{p0,j} \tag{16}$$

$$\frac{dQ(x)}{dx}|_j = h_f A_{rf}\alpha(T_{f0,j}(x) - T_{fm,j}(x)) = h_p A_{rp}\alpha(T_{pm,j}(x) - T_{p1,j}(x)) \tag{19a}$$

$$\frac{dQ(x)}{dx}|_j = h_p A_{rp}\alpha(T_{pm,j}(x) - T_{p1,j}(x)) = h_m A_{rln}\alpha(T_{fm,j}(x) - T_{pm,j}(x)) + N_{v,j}(x)\alpha(\Delta H_v(T_{pm,j}(x)) + C_{pm,j}T_{pm,j}(x)) \tag{19b}$$

Given the feed conditions of brine and distillate in the jth layer at x (i.e., flow rate and temperature), the values of $T_{fm,j}(x)$, $T_{pm,j}(x)$, $T_{p1,j}(x)$, $N_{v,j}(x)$, and $V_{p1,j}(x)$ can be calculated from the set of five equations above, along with the boundary condition $Q(0)|_j = 0$. These equations were solved using the Newton−Raphson method for $n \times n$ systems.[24] The values of other variables can be calculated correspondingly using appropriate relations.

Experimental Details

In our earlier studies,[17] details of the smaller crossflow modules having membrane surface areas based on internal diameter varying between 119 and 256 cm^2 have been provided. The most successful of the modules in terms of DCMD and VMD performance was MXFR#3 containing 180 fibers having an inner diameter-based surface area of 119 cm^2. The picture frame had inner dimensions of the crossflow modules which were 6.4 cm length × 2.5 cm width × 1.8 cm height. Two larger modules prepared for this study employed the same precursor hollow fiber membrane (330 μm i.d., 150 μm wall thickness from Membrana, Charlotte, NC) and a similar plasma polymerized silicone−fluoropolymer coating on the fiber outside surface. The picture frame dimensions were much larger (25.4 cm length × 8.57 cm width × 4.45 cm height); the total number of fibers was also much larger, e.g., 1008 fibers in modules S/N 1004 and S/N 1005. All fibers in each module in the consecutive layers were potted in a sort of staggered arrangement. Details are provided in Table 1. Figure 2 illustrates

Table 1. Details of Larger Hollow Fibers and Membrane Modules

Particulars	MXFR #3	S/N 1004	S/N 1005
support membrane type		PP 150/330	
fiber i.d., μm		330	
wall thickness, μm		150	
maximum pore size, μm		0.65	
membrane porosity		~0.6−0.8	
coating[a]		silicone fluoropolymer	
arrangement of fibers		staggered	
no. of fibers (no. of layers × fibers/layer)	10 × 18 = 180		16 × 68 = 1088
effective membrane surface area, cm^2 [b]	119		2864
effective cross-sectional area for shell-side liquid flow, cm^2 [c]	8.74		108.9
rectangular module frame (internal dimensions)	*L* 6.4 cm, *W* 2.5 cm, *H* 1.8 cm		*L* 25.4 cm; *W* 8.6 cm; *H* 4.45 cm
packing fraction of fibers	0.12		0.22
shell-side flow mode		crossflow	

[a] All coatings were applied on the outside diameter of the support fibers by Applied Membrane Technology, Inc., Minnetonka, MN, using their proprietary plasma polymerization technology. [b] Based on fiber internal diameter. [c] Based on open area for flow = frame cross-sectional area − fiber projected area (no. of fibers in one layer × fiber o.d. × length of fiber (cm^2)).

the relative dimensions of the picture frame of each module (MXFR#3, small) (S/N 1004, large) as received from Applied Membrane Technology, Minnetonka, MN.

The picture frame modules were only rectangular channels having coated hollow fibers running across them and two open faces; a diverging section and a converging section were designed and fabricated to allow the liquid to flow uniformly in crossflow outside of and perpendicular to the fibers. The diverging section and the converging section were two rectangular boxes having a curved shape (Figure 4a). Two face plates were made from two flat translucent polypropylene plastic sheets. On each sheet, 104 smaller holes having a wide size distribution were opened (the hole sizes were such that the holes at the center were smaller, while those further away were progressively larger) (Figure 4b). The design mentioned above attempted to ensure that the feed solution flowed uniformly through the shell side of the fibers.

Two face boxes and face plates were assembled with a rectangular membrane module channel and 10 bolts to constitute the complete device (Figure 4c). Neoprene gaskets ($^1/_8$ in.) were used between the face box, the face plate, and the module channel on each side to seal the parts together. Hot brine was allowed to enter one face box, then to leave the box through the face plate holes which distributed the liquid flow evenly, and then to enter the flow channel. On the other side, the liquid left the channel through the face plate holes, collected in the face box, and then flowed beyond the box and thus the module. In this design, between the face plate and the frame containing the fibers, there was space due to the gasket. Further, there was a small axial gap around $^1/_4$ in. between the module frame surface and the beginning of the fibers. This allowed evening out of any irregularity in the flow out of the face plate into the fibers. The liquid flow was expected to cross the fiber layer uniformly and perpendicularly to ensure good heat and mass transfer.

Experimental Apparatus and Procedure. A schematic of the experimental apparatus in terms of a process flow diagram is shown in Figure 5. All of the system piping and storage tanks were thoroughly insulated to minimize heat loss to the environment. In the experimental setup, city water or brine was introduced to the shell side from a reservoir by a centrifugal pump (model TE-4-MD−HC, Little Giant Co., Oklahoma City, OK) at a constant flow rate controlled by a ball valve. The flow rate of the liquid system could be varied between 5 and 40 LPM. Feed solution in a 200-L stainless steel tank was heated by a heating system having two heaters (OMEGA, EMT-312E2/240 three-phase moisture resistant heater (12 kW); EMT-309E2/240 three-phase moisture resistant heater (9 kW); a total 21 kW of heating capacity), two OMEGA rugged transition joint probes, two OMEGA three-phase DIN rail-mounted solid-state relays, and two OMEGA CN77333 controllers. The temperature controllers maintained the bath temperature at a given value and thus maintained a constant entrance temperature for the hot brine/water feed. Outside the membrane module, the exiting feed was circulated back to the feed reservoir and was rewarmed. For safety, a liquid level switch was installed in the feed tank.

The cooling system was mainly composed of a Remcor chiller having a cooling capacity of 12 kW (model CH3002A, voltage (full load amps) 230/60/3, IMI Cornelius Inc., Anoka, MN) with a recirculation pump and a 10 gallon tank. Deionized water was introduced as the cooling liquid on the fiber lumen side of the module from the reservoir at a constant flow rate. The exiting hot distillate from the module was cooled to a given temperature by the chiller before entering the module again. Each liquid solution (including feed solution and cooling water) was filtered by passing through a 20-in. postfilter cartridge (1 μm) (model DGD-2501−20, USFilter-Plymouth Products, Sheboygan, WI) before entering the membrane module.

The inlet and outlet temperatures and pressures of the hot feed and the cold distillate were measured by thermocouples and pressure gauges. The electrical conductivities or the salt concentrations of the distillate into and out of the module were monitored by a conductivity meter (model CON200 Series, OAKTON Instruments, Vernon Hills, IL).

When the readings of the flow rates of the hot solution, cold distillate water, and the four inlet and outlet temperatures reached constant values, it was assumed that the experimental conditions had reached a steady state; then, the distillate spilled from the cooling water reservoir beyond a certain level was collected. The volume of the distillate collected in a certain time was used to calculate the water vapor flux through the membrane under the given experimental conditions. Water vapor flux was calculated from the following relation:

$$\text{Water vapor flux}\left(\frac{\text{kg}}{\text{m}^2\,\text{h}}\right) = \frac{\text{volume of water transferred (L)} \times \text{density of water (kg/L)}}{\text{membrane area (m}^2\text{)} \times \text{time (h)}} \quad (20)$$

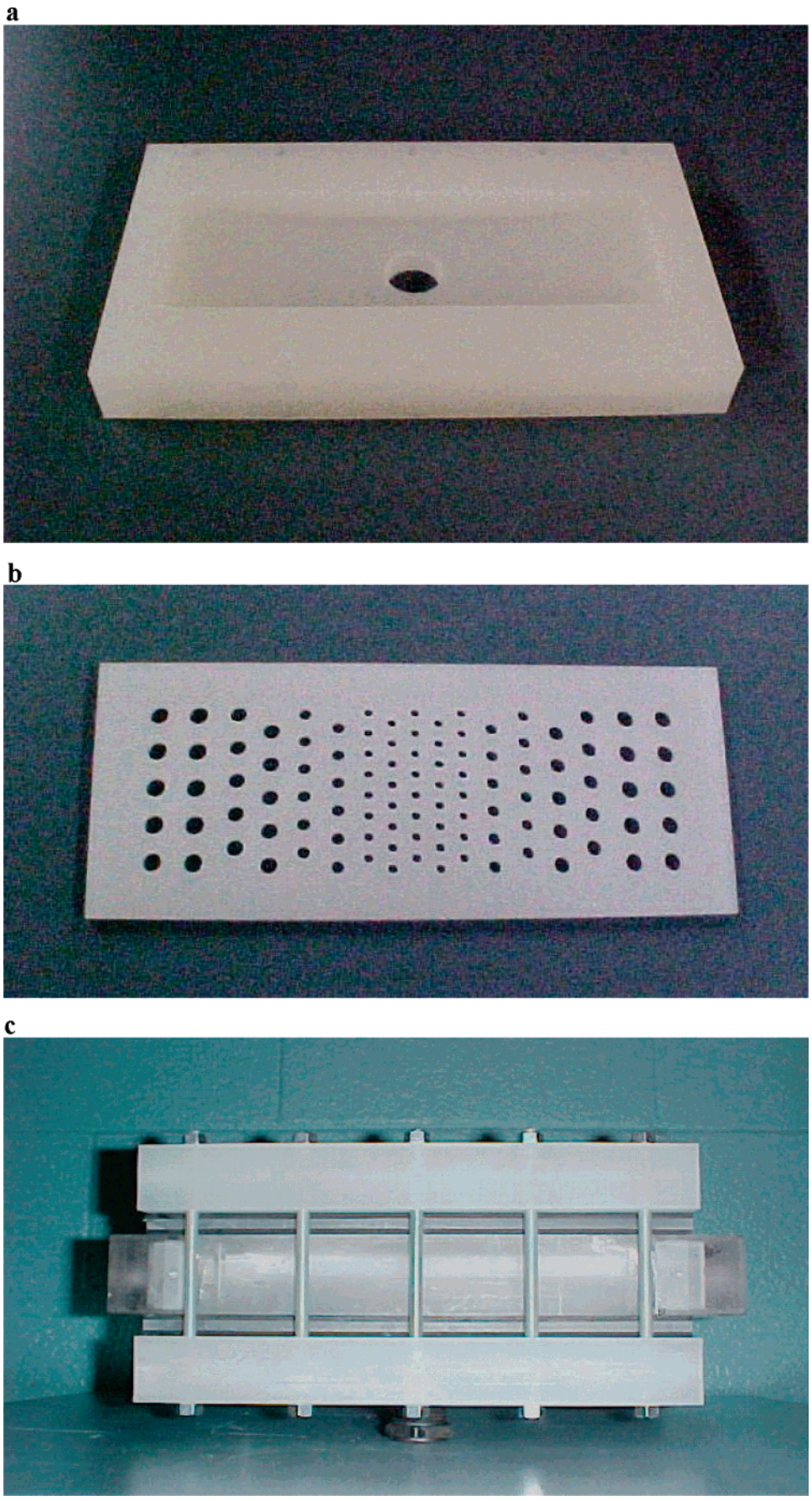

Figure 4. (a) Face box fabricated for larger-scale rectangular crossflow module. (b) Face plate fabricated for larger-scale rectangular crossflow module. (c) Larger-scale rectangular crossflow test module with face boxes, plates, and assembly.

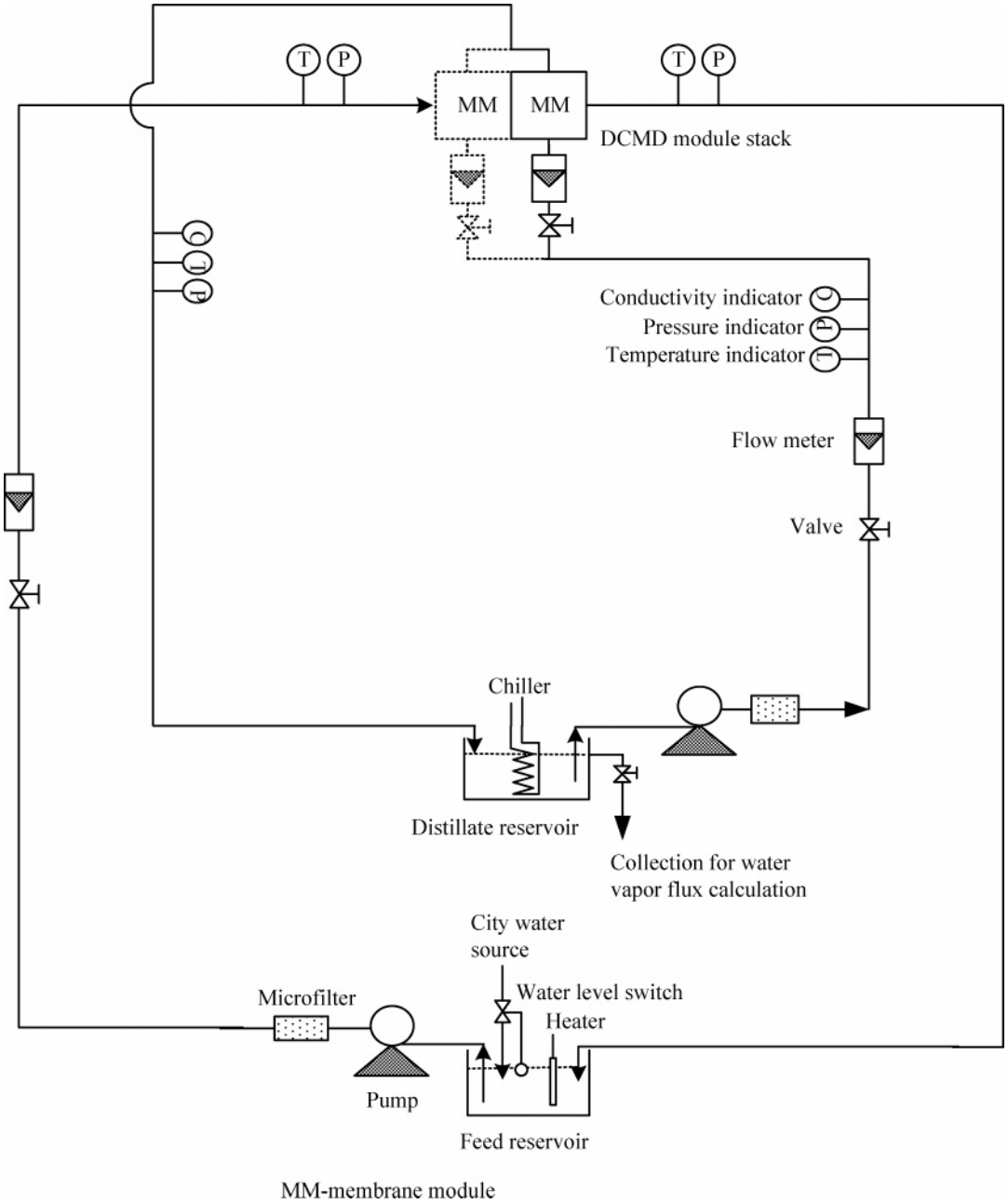

Figure 5. Process flow diagram for DCMD experimental setup.

Here, the membrane area was calculated based on the hollow fiber inside area, $s = nm\pi d_i L$, where n is the number of fibers in a given layer in a membrane module having m layers, d_i is the fiber inside diameter (i.d.), and L is the fiber length.

The larger membrane modules listed in Tables 1 were tested for leakage before DCMD measurements. Before the leak tests, each membrane module was activated by circulating deionized water in the shell side and tube side at a very low flow rate and at room temperature for at least 10 h. Then, the module was assembled in the DCMD system. A solution of 1% NaCl at 85 °C flowed through shell side at a constant flow rate of 5−25 LPM (the pressure drop was kept in the range of 1−2.5 psi (6.9−17.25 kPa)), and deionized water flowed through the tube side at a low flow rate at room temperature. The conductivity of the distillate was monitored with the increasing brine flow rate. If the conductivity of the distillate water rose evidently with operating time, the test membrane module was leaking. Otherwise, the test membrane module was leak-free. Besides, filling deionized water in the tube side and keeping a constant pressure for a long time is another way to check the leakage status of a hollow fiber module.

The Reynolds number is normally defined in the following way:

$$Re = \frac{Du\rho}{\mu} \tag{21}$$

Here, Re is the Reynolds number; D is the characteristic dimension; u is the velocity; ρ is the density; and μ is the dynamic viscosity (absolute viscosity). The Reynolds numbers of the hot feed or the cold distillate flowing through the shell or the tube side were defined as diameter-based Reynolds number (Re_d). In the calculation of Re_d based on eq 21, fiber i.d. (d_i) and linear velocity are used for tube-parallel flow and fiber o.d. and interstitial velocity are use for shell-side crossflow;

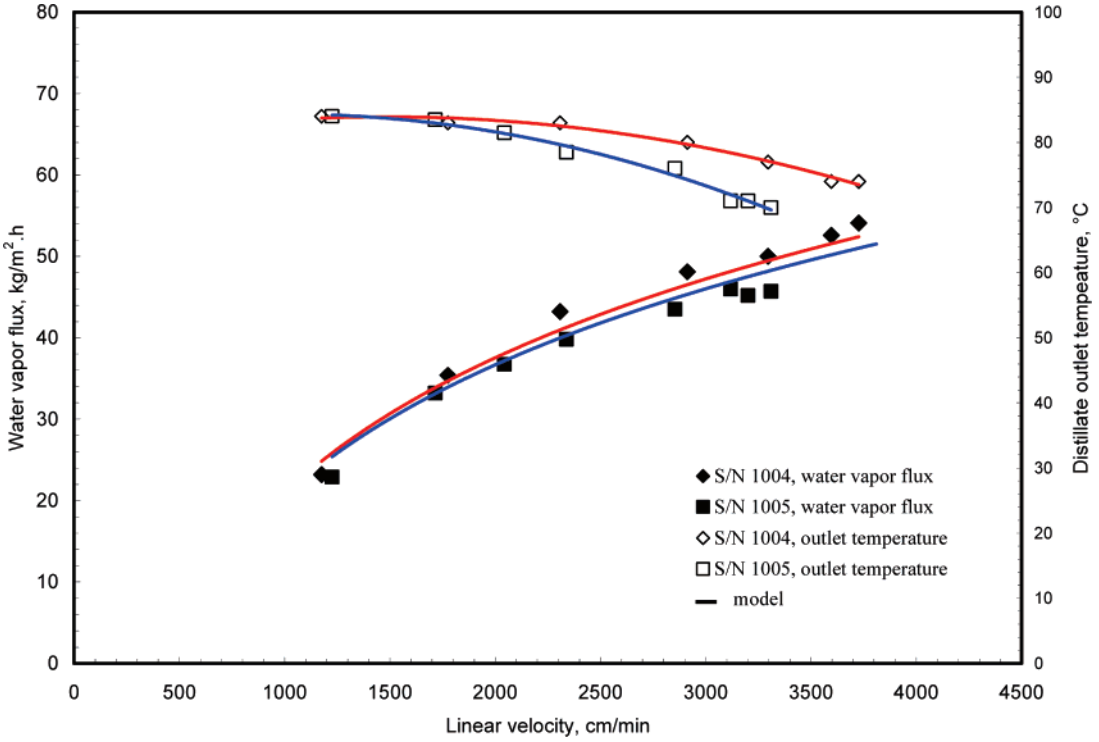

Figure 6. Comparison of DCMD performance of modules S/N 1004 and S/N 1005: variation of water vapor flux and outlet temperature of the distillate with the inlet linear velocity of the distillate flowing through the tube side at inlet temperatures of 16−24 °C and 3% brine at 85 °C flowing on the shell side at 25 LPM (interstitial velocity of 230 cm/min).

the highest interstitial velocity achievable was around 240 cm/min:

$$\text{Interstitial velocity } (u_I) = \text{brine flow rate/open area for flow through the shell side} \quad (22)$$

The open area for flow through the shell side has been defined at the bottom of Table 1.

$$\text{Linear velocity } (u_L) = \text{flow rate/open area for flow through the tube side} \quad (23)$$

Results and Discussion

We will first present the DCMD performance results obtained using the two larger modules S/N 1004 and S/N 1005. The performance of the membrane module S/N 1004 was studied as a function of the hot brine inlet temperature, the feed salt concentration, tube-side linear velocity of the distillate, and the distillate inlet temperature. The quantity of prime interest here was the water vapor flux obtained from the module. An additional quantity of interest was the distillate outlet temperature; the performance of the membrane module S/N 1005 was also studied to those ends, and the results were compared with those from the module S/N 1004. Next, we will present the results of an extended continuous DCMD run for module S/N 1004 lasting 5 days. After these experimental results are presented, we will focus on the predictions from the model developed here. We will test the utility of the model using not only the data from the larger MD modules of this study but also the much smaller module MXFR#3 of the earlier study.[17] We will then focus on some other predictive features of the model presented here.

Large Rectangular Crossflow Hollow Fiber Membrane Modules. Two rectangular crossflow membrane modules, namely, S/N 1004 and S/N 1005 described in Table 1, were used for DCMD measurements. In Figure 6, the effect of linear velocity of the distillate on the water vapor flux was investigated for both modules. It can be seen that the distillate outlet temperature decreased with an increase of linear velocity of the distillate due to the decrease of the residence time of the distillate in the module, which led to an increase of the driving force for water vapor permeation due to increasing $\Delta T = T_{\text{brine}} - T_{\text{distillate}}$. This led to a higher water vapor flux. Also, an increase of the linear velocity in parallel flow on the tube side led to an increase of the Reynolds number which maximized the distillate-side boundary layer heat transfer coefficient. The higher heat transfer coefficient leads to a lower temperature at the distillate−membrane interface which supports the increased water vapor flux.

We observed in module S/N 1004 a water vapor flux value of around 54 kg/(m^2 h), the level achieved with an orders of magnitude smaller module, MXFR#3, in our earlier study,[17] when the linear distillate velocity was 3900 cm/min. However, the water vapor flux of the larger module is somewhat lower than that of small module MXFR #3. The larger module has an effectively lower ΔT due to the distillate getting heated up along the much longer fibers. We also notice that, at a low linear velocity of the distillate in the fiber lumen, e.g., 1200 cm/min, the outlet temperature of the distillate reached 84 °C which means that there was essentially no temperature difference across the membrane since the feed inlet and outlet temperatures were between 84.5 and 85 °C. Even if the distillate linear velocity was as high as 3800 cm/min, the distillate outlet temperature still was 74 °C or higher for module S/N 1004. The module S/N 1005 appears to have a marginally lower performance than the module S/N 1004.

A variation of the water vapor flux with feed inlet temperature is illustrated in Figure 7 for city water, 3% brine, 6% brine, and 10% brine. Normally, the feed temperature has a small effect on the Reynolds number at a given flow rate since there are only limited changes in the density and the viscosity of water

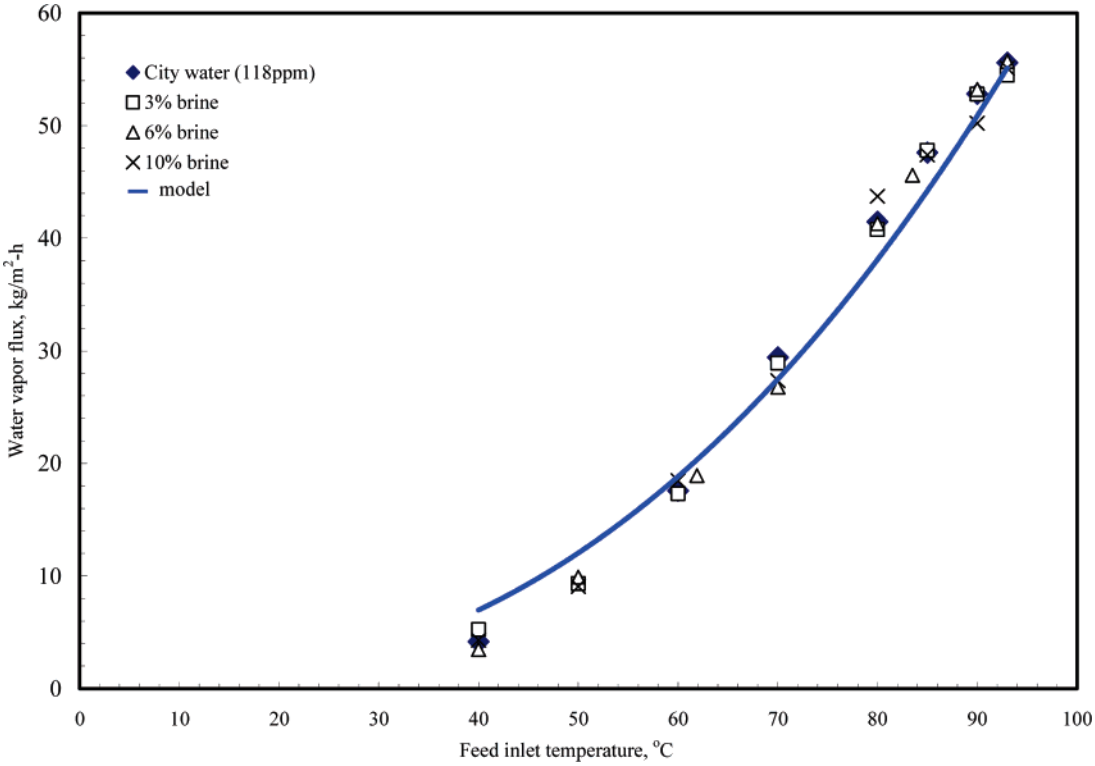

Figure 7. DCMD performance of module S/N 1004 with city water, 3% brine, 6% brine, and 10% brine as feed solutions: variation of water vapor flux with feed inlet temperature: (shell side) brine solution at 230 cm/min of interstitial velocity; (tube side) distillate at 2850 cm/min of average linear velocity at 25−35 °C of the inlet temperature.

in the given temperature range. But, the effect of temperature on the water vapor permeation flux is striking. The increase of the feed temperature increases the Reynolds number a little bit, but it drastically increases the water vapor pressure which is the driving force. The water vapor flux rises almost exponentially with temperature as the brine temperature rises.

It is important to know how the DCMD membrane system works with different brine solutions as feed under the current experimental conditions. It is expected that the effect of salt concentration for dilute solutions over this performance is going to be minor. It is also necessary to investigate the membrane behavior working with more highly concentrated salt solutions under DCMD conditions for testing its overall usefulness. A group of DCMD experiments was conducted to determine the effect of NaCl concentration on the water vapor flux in the large rectangular crossflow membrane modules. The experimental data shown in Figures 7 and 8 do not provide any conclusive evidence that increasing the NaCl concentration of the feed to 10% of NaCl reduces the system performance too much. This is obvious since water vapor pressure is affected to a small extent by salt concentration, which can be explained by using eqs 17a, 17b, 18a, and 18b. When the salt concentration in water is 10%, $p_{water}/p^0_{water} = 0.94$; when the salt concentration reaches 20%, $p_{water}/p^0_{water} = 0.85$. The crossflow of hot feed on the shell side is also a very important contributing factor which could reduce the temperature polarization to a great extent. These results point out that DCMD may be used to successfully recover water at a high rate from highly concentrated salt solutions, e.g., the rejected hot seawater/the hot brine blowdown from a thermal distillation plant (unless scaling is problematic). It also suggests how the concentrate volume from existing water desalination plants may be reduced and more water recovered.

Figure 9 illustrates how the distillate inlet temperature affects the DCMD performance of module S/N 1004. The water vapor flux obtained has been plotted for a 3% brine feed at 91−93 °C flowing on the shell side at an interstitial velocity of 230 cm/min and distillate flowing on the tube side at a linear velocity of 2950 cm/min as a function of the distillate inlet temperature. As the inlet distillate temperature is increased, the driving force of the DCMD process is decreased and therefore the water vapor flux decreases. It can be seen during this experiment that the distillate outlet temperature was just raised by 4 °C (from 88 to 92 °C, very close to the feed inlet temperature) even as the distillate inlet temperature was varied between 30 and 60 °C. This indicates that an even higher water vapor flux in the future may be obtained by optimizing the experimental operations even though the water vapor flux has already reached 56.5 kg/(m^2 h). We also found that a very high water vapor flux of 42 kg/(m^2 h) was obtained although the inlet temperature of distillate was as high as 55 °C.

DCMD Experiments for an Extended Period. Membrane module S/N 1004 was employed for an extended DCMD run where a feed of 3% hot brine was circulated through a microfilter, the shell side of module S/N 1004, and the feed reservoir. Similarly, cold distillate (DI) water was recirculated as the distillate stream through a microfilter, the lumen, the distillate reservoir, and the thermostat shown in Figure 5. Figure 10 represents the variation of the water vapor flux with the operating time. For a brine feed at a temperature of 87−90 °C, this experiment lasted 5 days. The water vapor flux of the membrane dropped very slowly as the experiment was run for 100 h. The stable water vapor flux was 54 kg/(m^2 h). There was a reduction of only 6% in the water vapor flux. Compared to the membrane module MXFR #3[17] (a reduction of 23% during the 5-day long-term experiment), the 6% reduction is much smaller. Although the role of the thermal creep in the membrane and coating material with time around the mouth of the partially covered pore at a high temperature cannot be eliminated, the fouling of the membrane both on the shell-side and tube-side surfaces was inhibited effectively by microfiltration (1 μm). The

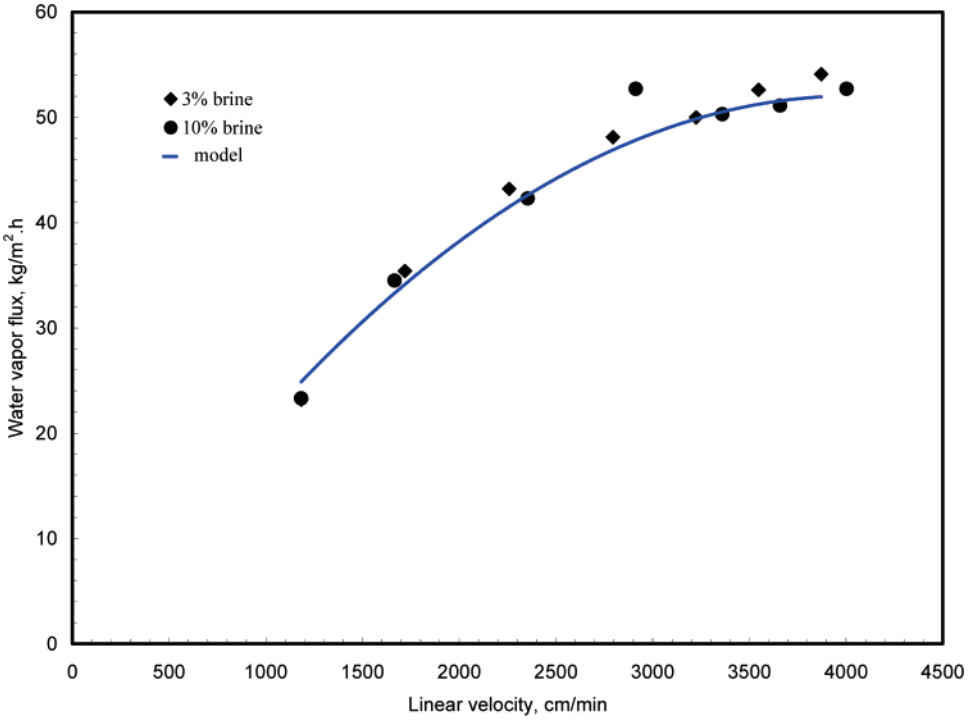

Figure 8. DCMD performance of module S/N 1004 (membrane surface area 2864 cm^2) with 3% brine and 10% brine as feed solutions: variation of water vapor flux with linear velocity of distillate flowing through the tube side at inlet temperatures of 18−26 °C and hot brine flowing on the shell side with 25 LPM (interstitial velocity of 230 cm/min) at a temperature of 85−88 °C.

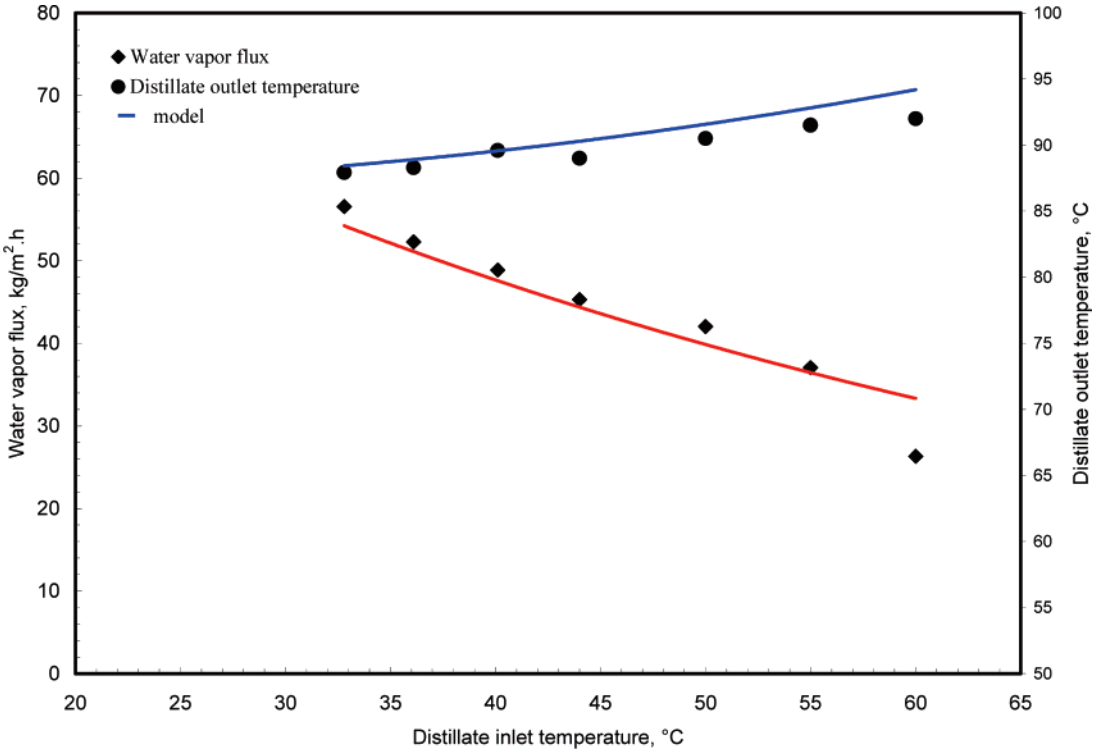

Figure 9. DCMD performance of module S/N 1004 (membrane surface area 2864 cm^2): variation of water vapor flux with distillate inlet temperature: (shell side) 3% brine at 230 cm/min of interstitial velocity at a temperature of 91−93 °C; (tube side) distillate at 2950 cm/min of linear velocity. The variation of the distillate outlet temperature with the distillate inlet temperature has also been shown.

conductivity of the cold distillate was monitored during this extended experiment. The concentration of salt was always less than 10 mg/L, which indicates that the membrane pores were not wetted by the hot brine during this experiment. No bacterial stain was observed in the membrane module or the brine reservoir during the 5-day experiment. Generally, bacterium cannot grow in water at a temperature over 85 °C. However, the pressure drop in the cold distillate water passing through the lumen side of the module was slightly increased (by 8%). This indicates the possibility of dirt buildup in the hollow fiber tube sheet.

A note about the mode of operation during the long-term test is in order. The experiments were started in the morning at 8 am with 87−90 °C brine feed on the first day; then, at about 8 pm in the evening, the hot feed temperature was reduced to 50 °C. The next morning at 8 am, the hot feed temperature was

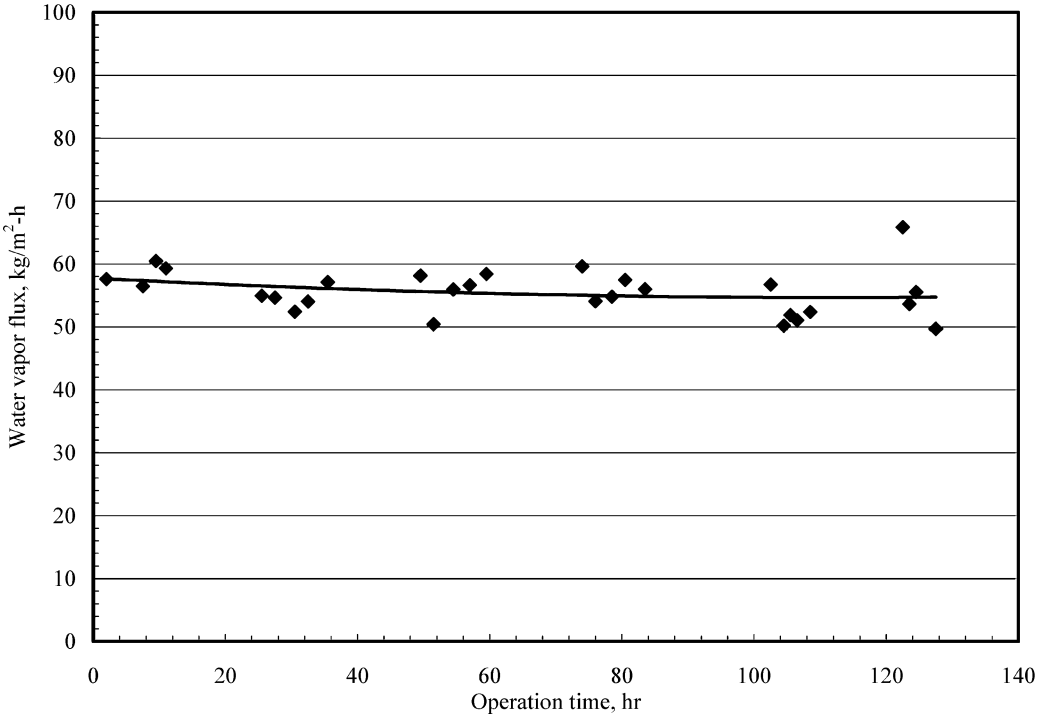

Figure 10. DCMD: Variation of water vapor flux with operating time for hot brine (3% NaCl) recirculating through the shell side with an inlet velocity of 253 cm/min (Reynolds number, 78) at 87−90 °C and cold distillate water recirculating through tube side at an inlet velocity of 3870−4060 cm/min (Reynolds number, 448−471) at an inlet temperature of 34−42 °C (module S/N 1004).

increased again to 87−90 °C; at 8 pm in the evening, the hot feed temperature was reduced again to 50 °C. The water vapor fluxes reported correspond to the high-temperature feed during the first 12 h of the day during the 5-day period. The brine Reynolds number employed was 78.

Membrane module S/N 1004 was used for a cumulative time of around 300 h since the beginning of the study and continuously over a period of 5 days/127 h. No leakage was observed. The silicone−fluoropolymer coating appears to provide an effective barrier to protect the membrane. The membrane performance demonstrated very good stability and also indicated that this scaled-up module can perform as well as the much smaller module MXFR #3 both in terms of water vapor flux and distillate water quality.

Model Results. Solution of the five eqs 13a, 13b, 14, 16, 19a, and 19b can be carried out using the input values V_{b0}, T_{b0}, V_{d0}, and T_{d0} and details of the module geometry and fiber dimensions and properties. Of the latter, the values of the thermal conductivities, k_{mg} and k_{ms}, are 0.03 W/(m K)[25] and 0.17 W/(m K)[26], respectively. However, the value of the membrane water vapor mass transfer coefficient k_m is an unknown. Li and Sirkar[18] had developed an estimate of k_m for the module MXFR#3 from VMD measurements. The conditions for DCMD measurement, especially the presence of air in the pores and different temperature profiles along the pore length, suggest that k_m in DCMD will be somewhat different. We have therefore used k_m as the only adjustable parameter here. The values assumed are:

$$\text{S/N 1004 and S/N 1005} \rightarrow k_m = 0.0022 \text{ kg/(m}^2 \text{ h Pa)}$$

$$\text{MXFR\#3} \rightarrow k_m = 0.0018 \text{ kg/(m}^2 \text{ h Pa)}$$

Note that Li and Sirkar[18] had found a value of k_m not too far from these values.

The results of simulations for the water vapor flux obtained in the two larger modules S/N 1004 and S/N 1005 are shown in Figure 6 as solid lines. It appears that the model predictions are reasonably close to the observed variation of the water vapor flux with the distillate flow velocity variation. The predictions of the distillate outlet temperature as a function of the distillate velocity variation also appear to describe the observed data well. The simulations for the water vapor flux for three different salt concentrations in the larger module S/N 1004 as a function of brine feed temperature (Figure 7) illustrate (as does the experimental data) that the increased salt concentration has a very minor effect on the observed/predicted water vapor flux, a distinct strength of DCMD/VMD processes. The same behavior, namely, a very limited effect of the salt concentration (3% and 10%) on the observed water vapor flux as a function of the distillate linear velocity is predicted in Figure 8.

The strong effect of an increased distillate inlet temperature on the reduction of the water vapor flux and rise in the distillate outlet temperature are predicted by the model as well for the module S/N 1004 as shown in Figure 9. We know that as the feed brine temperature is increased, the water vapor flux is increased (Figure 7). The model predicts such a behavior reasonably well for the smaller module (MXFR#3) also for two different brine velocities (Figure 11).

In the next three figures (Figures 12−14), the predictive ability of the model for the extensive data collected with both modules S/N 1004 and MXFR#3 are tested. Figure 12 tests this vis-à-vis the experimentally observed shell-side outlet temperature. We note that generally the model is able to predict these values well over a temperature range varying between 30 and 90 °C. There is some scatter especially with the data from the smaller module. Figure 13 shows that the model can predict the values of the tube-side distillate outlet temperature over a wide range, 30−90 °C. However, the scatter appears to be somewhat larger. There is an overprediction at lower temperatures and underpredicton at higher temperatures. This suggests that, perhaps among other strategies, we need to test other heat transfer coefficient correlations for the tube side. The scatter as

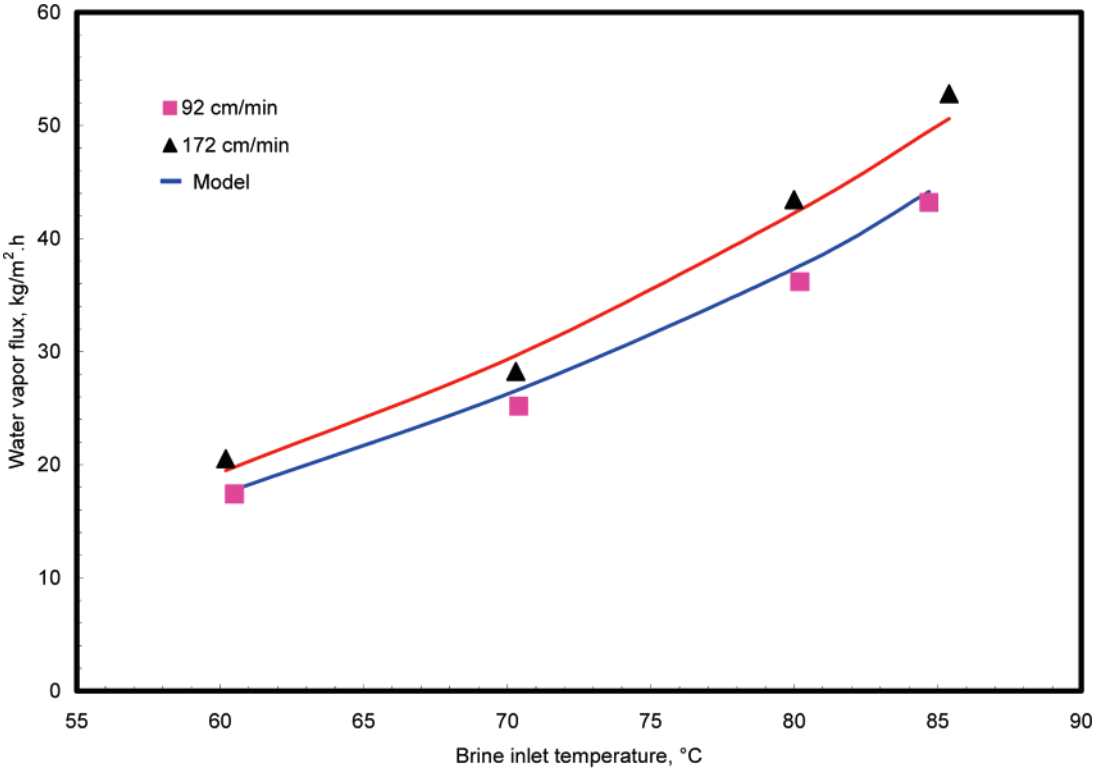

Figure 11. DCMD performance of module MXFR#3 (membrane surface area 119 cm^2): variation of water vapor flux with inlet temperature of hot brine (1% NaCl) as feed flowing on the shell side (crossflow) at various interstitial velocities (tube side, 15−17 °C DI water, linear velocity 1660 cm/min).

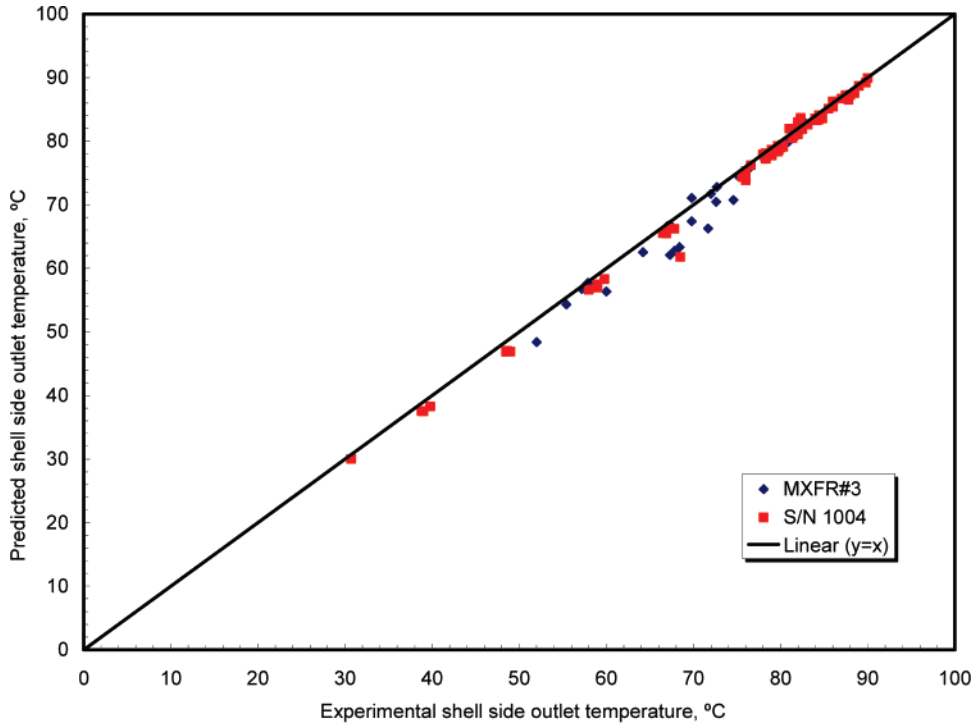

Figure 12. Comparison of predicted shell-side brine outlet temperatures with DCMD experimental data for modules MXFR#3 and S/N 1004: (running conditions for MXFR#3) 1% NaCl solution, shell-side brine feed rate 200−2281 mL/min (interstitial velocity 23−261 cm/min), brine feed temperature 30.8−93.8 °C, tube-side distillate (deionized water) feed rate 112−600 mL/min (linear velocity 727−3900 cm/min), distillate feed temperature 12.5−22.4 °C; (running conditions for S/N 1004) city water or 3−10% NaCl solution, shell-side brine feed rate 5000−33 000 mL/min (interstitial velocity 46−303 cm/min), brine feed temperature 30.8−93.8 °C, tube-side distillate feed rate 1096−4092 mL/min (linear velocity 1264−4400 cm/min), distillate feed temperature 18.3−60 °C.

shown in Figure 14 for the water vapor flux values is larger. The range of water vapor flux values covered here is however broad: 4−5 to 60 kg/(m^2 h). The question of whether one k_m can be used over a wide range of temperatures for such predictions is crucial here. It will be an item of our future focus.

The remaining figures on modeling results (Figures 15−18) will focus on model predictions regarding the performance variation along the fiber length, the module depth, as well as the temperature polarization for the module MXFR#3. Figure 15 points out that as the hot feed brine hits the first layer of

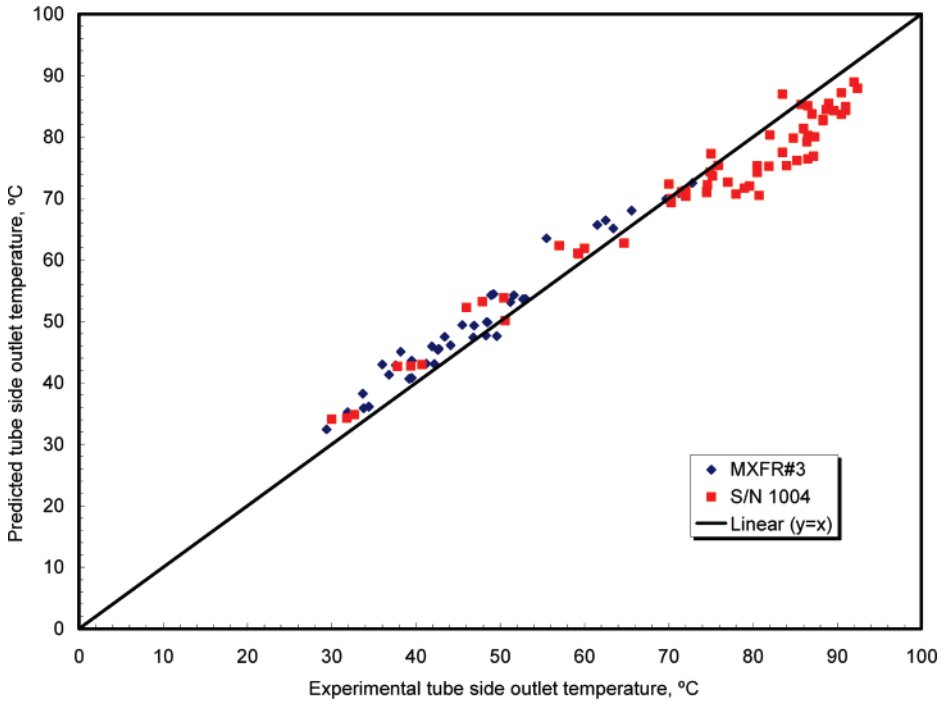

Figure 13. Comparison of predicted tube-side distillate outlet temperatures with DCMD experimental data for modules MXFR#3 and S/N 1004: (running conditions for MXFR#3) 1% NaCl solution, shell-side brine feed rate 200−2281 mL/min (interstitial velocity 23−261 cm/min), brine feed temperature 30.8−93.8 °C, tube-side distillate (deionized water) feed rate 112−600 mL/min (linear velocity 727−3900 cm/min), distillate feed temperature 12.5−22.4 °C; (running conditions for S/N 1004) city water or 3−10% NaCl solution, shell-side brine feed rate 5000−33 000 mL/min (interstitial velocity 46−303 cm/min), brine feed temperature 30.8−93.8 °C, tube-side distillate feed rate 1096−4092 mL/min (linear velocity 1264−4400 cm/min), distillate feed temperature 18.3−60 °C.

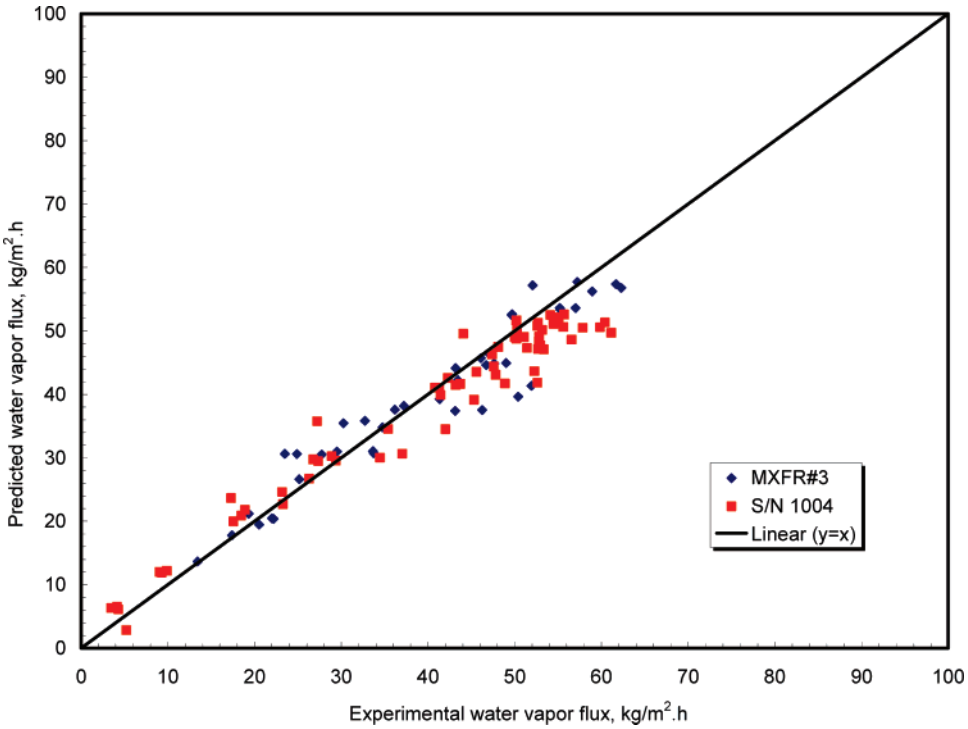

Figure 14. Comparison of predicted water vapor flux with DCMD experimental data for modules MXFR#3 and S/N 1004: (running conditions for MXFR#3) 1% NaCl solution, shell-side brine feed rate 200−2281 mL/min (interstitial velocity 23−261 cm/min), brine feed temperature 30.8−93.8 °C, tube-side distillate (deionized water) feed rate 112−600 mL/min (linear velocity 727−3900 cm/min), distillate feed temperature 12.5−22.4 °C; (running conditions for S/N 1004) city water or 3−10% NaCl solution, shell-side brine feed rate 5000−33 000 mL/min (interstitial velocity 46−303 cm/min), brine feed temperature 30.8−93.8 °C, tube-side distillate feed rate 1096−4092 mL/min (linear velocity 1264−4400 cm/min), distillate feed temperature 18.3−60 °C.

fibers, the distillate starts getting heated up; as a result, the water vapor flux is reduced along the fiber length and the brine is cooled down to a lesser extent. Correspondingly as we go down the fiber bed, we observe that the feed brine near the exit of the distillate stream is considerably warmer than that near the distillate stream entrance. This is a direct result of the assumption of no lateral brine-side mixing in our model. Figure 16 is focused on temperature polarization in the feed brine region as well as in the distillate fiber bore for the first layer of fibers. As expected, the extent of temperature polarization on the brine

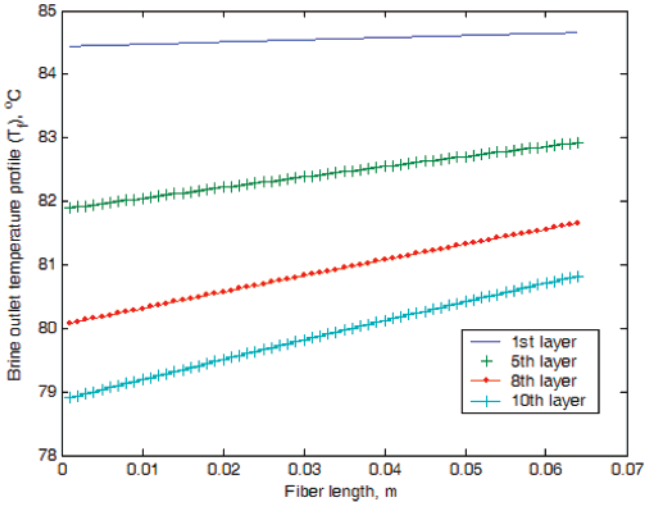

Figure 15. Variation of local temperature profiles of brine bulk temperature along the fiber length for different fiber layers in DCMD module MXFR#3: shell-side flow rate 2000 mL/min, interstitial velocity 229 cm/min, inlet temperature 85.1 °C; tube-side flow rate 400 mL/min, linear velocity 2600 cm/min, inlet temperature 19.8 °C.

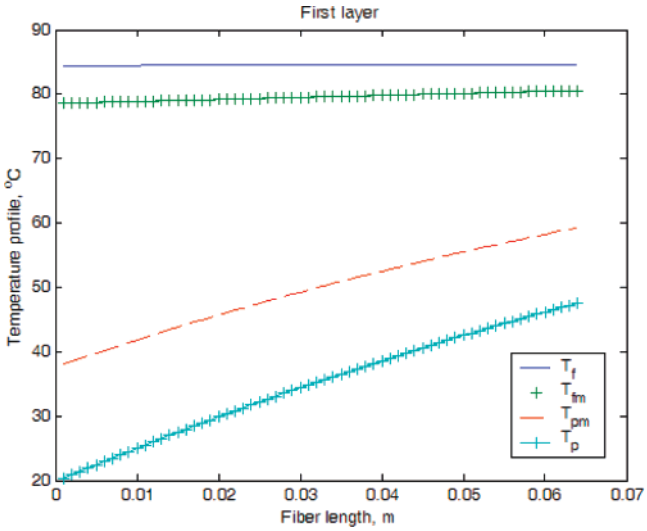

Figure 16. Variation of local temperature profiles of brine bulk temperature, wall temperature on the fiber outside surface, wall temperature on the fiber inside surface, and distillate bulk temperature along the fiber length for the first fiber layer in DCMD module MXFR#3: shell-side flow rate 2000 mL/min, interstitial velocity 229 cm/min, inlet temperature 85.1 °C; tube-side flow rate 400 mL/min, linear velocity 2600 cm/min, inlet temperature 19.8 °C.

side with efficient crossflow-based heat transfer is considerably less than that in the distillate tube side. We observe a similar temperature polarization behavior in Figure 17 for the 10th layer of fibers in module MXFR#3.

The result of a significant rise in distillate temperature along the fiber length will lead to a reduction in the local water vapor flux. This strong reduction in local water vapor flux with fiber length along the distillate flow direction is illustrated in Figure 18 for four layers of fibers in the small module MXFR#3. Such a flux reduction will reduce the brine temperature drop with fiber length leading to hotter brine near the distillate outlet as we have observed earlier in Figure 15. These modeling results suggest that additional considerations are needed to exploit such observed behavior to beneficial ends in multimodule cascades for the DCMD process.

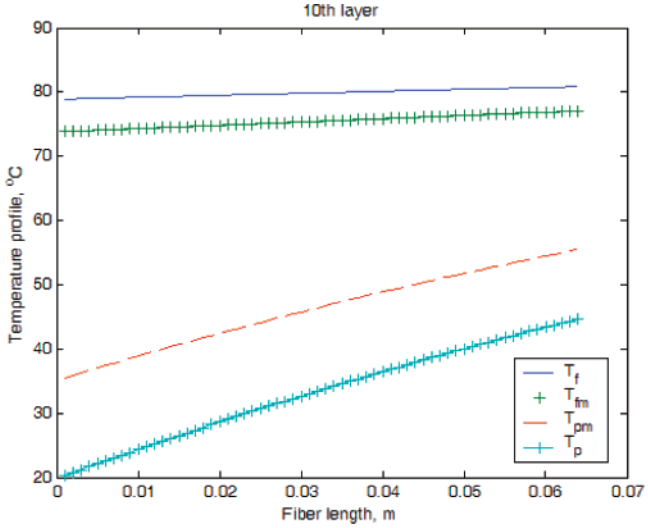

Figure 17. Variation of local temperature profiles of brine bulk temperature, wall temperature on the fiber outside surface, wall temperature on the fiber inside surface, and distillate bulk temperature along the fiber length for the tenth fiber layer in DCMD module MXFR#3: shell-side flow rate 2000 mL/min, interstitial velocity 229 cm/min, inlet temperature 85.1 °C; tube-side flow rate 400 mL/min, linear velocity 2600 cm/min, inlet temperature 19.8 °C.

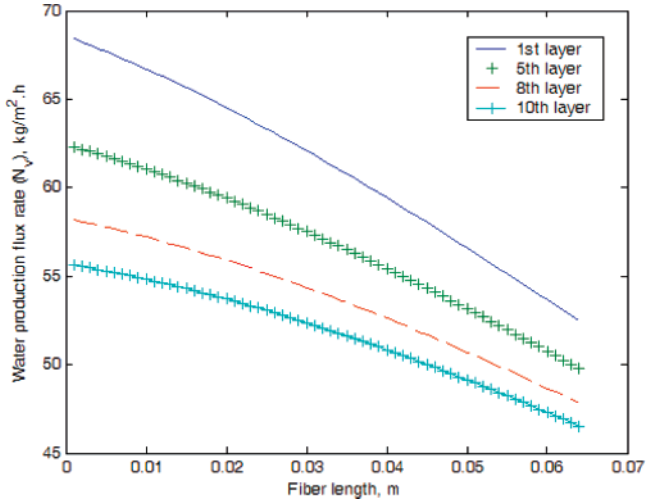

Figure 18. Variation of local water vapor flux along the fiber length for the tenth fiber layer in DCMD module MXFR#3: shell-side flow rate 2000 mL/min, interstitial velocity 229 cm/min, inlet temperature 85.1 °C; tube-side flow rate 400 mL/min, linear velocity 2600 cm/min, inlet temperature 19.8 °C.

Concluding Remarks

Two larger rectangular crossflow hollow fiber modules each having a membrane surface area of 0.2864 m^2 were experimentally investigated for their DCMD performance with synthetic NaCl-containing brine solutions. The salt concentrations studied were the following: city water and 3%, 6%, and 10% NaCl. The brine temperature was varied between 40 and 90 °C. The distillate temperature was varied between 32 and 60 °C; the distillate flow rate was varied over a broad range. The hollow fiber substrates were identical to those employed in Li and Sirkar;[17,18] the plasmapolymerized fluorosilicone coatings on their outside surface were quite similar.

The larger modules' DCMD performance was quite satisfactory. The water vapor flux levels were close to those obtained with much smaller modules (119 cm^2) with due allowances for distillate temperature rise through the much longer hollow fibers (25.4 vs 6.4 cm). Reasonable water vapor fluxes were obtained

even though the distillate inlet temperature was as high as 55−60 °C. The reduction in water vapor flux as NaCl content was increased up to 10% was very limited compared to that with city water. The 5-day long extended test demonstrated stable flux performance at around 55 kg/(m^2 h). The model developed describes the observed performances of both the larger and the smaller modules satisfactorily suggesting among others that Žukauskas' equation is quite useful for describing the shell-side brine flow heat transfer coefficient. Hot brine temperature drop, distillate temperature rise, and the average water vapor flux from the modules were predicted satisfactorily for the whole range of variables studied. Scaling up of the module from the small MXFR#3 to the much larger S/N 1004/1005 appears to be successful. Further modeling studies should focus on three items: lateral mixing effects if any on the hot brine flow in the shell side; testing various correlations for the tube-side heat transfer coefficient; the nature of variation of the membrane mass transfer coefficient k_m in the two-dimensional module environment.

Acknowledgment

The first three authors acknowledge funding for this experimental and theoretical research from the Desalination and Water Purification Research and Development Program of the Bureau of Reclamation, Denver, CO, under the following two contracts 02-FC-81-0840 and 04-FC-81-1037. They would also like to acknowledge the useful comments of Frank Leitz (Bureau of Reclamation). J.L.G. was supported during his sabbatical at NJIT by ONR award No. N000140510803 which allowed him to assist L.S. in the modeling activity.

Notation

A_{rf} = membrane area ratio for heat transfer through fiber outside surface, = d_o/d_i
A_{rln} = membrane area ratio for heat/mass transfer through the fiber based on logarithmic mean diameter-based surface, = d_{lm}/d_i
A_{rp} = membrane area ratio for heat transfer through fiber inside surface, = d_i/d_i
C_p = heat capacity, J/(kg K)
DCMD = direct contact membrane distillation
d_i = fiber inside diameter, m
d_{lm} = logarithmic mean diameter of fiber, m
d_o = fiber outside diameter, m
F_c = correction factor
h_f = shell-side feed heat transfer coefficient, W/(m^2 K)
h_m = membrane heat transfer coefficient, W/(m^2 K)
h_{mg} = heat transfer coefficient across the membrane pore gas phase, W/(m^2 K)
h_{ms} = heat transfer coefficient for the solid polymeric matrix, W/(m^2 K)
h_p = tube-side heat transfer coefficient, W/(m^2 K)
ΔH_v = heat of vaporization of water, J/kg
k_m = membrane mass transfer coefficient, kg/(m^2 h Pa)
k_{mg} = thermal conductivity of the gas phase, W/(m K)
k_{ms} = thermal conductivity of the matrix material, W/(m K)
L = fiber total length, m
m = number of fiber layers
MD = membrane distillation
MSF = multistage flash
n = fiber number per layer
Nu = Nusselt number
N_v = water vapor flux, kg/(m^2 h)
p = vapor pressure
p_{fm} = water vapor partial pressure at the membrane surface on the shell side, Pa
p^0_{fm} = vapor pressure of water at the membrane surface on the shell side, Pa
p_{pm} = water vapor partial pressure at the membrane surface on the tube side, Pa
p^0_{pm} = vapor pressure of water at the membrane surface on the tube side, Pa
Pr = Prandtl number, = $C_p\mu/k$
Δp_{br} = breakthrough pressure
Q = heat transfer rate, W
Re = Reynolds number
RO = reverse osmosis
T_{b0} = brine feed temperature, °C
T_{d0} = distillate feed temperature, °C
T_{d1} = distillate outlet temperature, °C
T_f = brine bulk temperature
T_{f0} = brine feed temperature, °C
T_{fm} = brine temperature at the membrane surface, °C
T_p = distillate bulk temperature
T_{p0} = distillate feed temperature for one layer, °C
T_{p1} = distillate outlet temperature for one layer, °C
T_{pm} = distillate temperature at the membrane surface, °C
u_I = interstitial velocity on shell side, m/s
u_L = linear velocity on tube side, m/s
V_{b0} = brine inlet volumetric flow rate, m^3/h
V_{b1} = brine outlet volumetric flow rate, m^3/h
V'_{f0} = local brine inlet volumetric flow rate per unit length of fiber, m^3/(h m)
V'_{f1} = local brine outlet volumetric flow rate per unit length of fiber, m^3/(h m)
VMD = vacuum membrane distillation
V_{d0} = distillate inlet volumetric flow rate, m^3/h
V_{d1} = distillate outlet volumetric flow rate, m^3/h
V_{p0} = distillate inlet volumetric flow rate for one fiber layer, m^3/h
V_{p1} = distillate outlet volumetric flow rate for one fiber layer, m^3/h
x = position along the fiber length, m, and water mole fraction

Greek Letters

α = membrane surface area based on fiber inside diameter per unit length per fiber layer
γ = activity coefficient
ϵ_m = membrane porosity
μ = viscosity, (Pa s)
ρ = density, kg/m^3

Subscript

0 = inlet (flow rate, temperature, density, heat capacity)
1 = outlet (flow rate, temperature, density, heat capacity)
b = brine
d = distillate
f = brine or shell side
i = distillate or fiber lumen side
j = the jth fiber layer
m = liquid−vapor interfaces on the brine side and distillate side
o = brine or shell side

p = distillate or fiber lumen side
w = wall or membrane surface

Literature Cited

(1) Findley, M. E. Vaporization through porous membranes. *Ind. Eng. Chem. Process Des. Dev.* **1967**, *6* (2), 226.

(2) Gore, D. W. Gore-Tex membrane distillation. In *Proceedings of the 10th Annual Convention of Water Supply Improvement Association*, Honolulu, Hawaii, July 25−29, 1982.

(3) Schofield, R. W.; Fane, A. G.; Fell, C. J. D. Heat and mass transfer in membrane distillation. *J. Membr. Sci.* **1987**, *33*, 299−313.

(4) Schneider, K. Hölz, W.; Wollbeck, R. Membranes and modules for transmembrane distillation. *J. Membr. Sci.* **1988**, *39*, 25−42.

(5) Sirkar, K. K. Other New Membrane Processes. In *Membrane Handbook*; Ho, W. S., Sirkar, K. K., Eds.; Van Nostrand Reinhold: New York, 1992; Chapter 46.

(6) Lawson, K. W.; Lloyd, D. L. Membrane distillation. *J. Membr. Sci.* **1997**, *124*, 1−25.

(7) Schofield, R. W.; Fane, A. G.; Fell, C. J. D. Gas and vapor transport through microporous membranes. I. Knudsen-Poiseuille transition. *J. Membr. Sci.* **1990**, *53*, 159−171.

(8) Schofield, R. W.; Fane, A. G.; Fell, C. J. D. Gas and vapor transport through microporous membranes. II. Membrane distillation. *J. Membr. Sci.* **1990**, *53*, 173−185.

(9) Schofield, R. W.; Fane, A. G.; Fell, C. J. D.; Macoun, R. Factors affecting flux in membrane distillation. *Desalination* **1990**, *77* (1−3), 279−294.

(10) Martinez-Diez, L.; Vazquez-Gonzalez, M. I. Temperature polarization in mass transport through hydrophobic membranes. *AIChE J.* **1996**, *42* (7), 1844−1852.

(11) Martinez-Diez, L.; Florido-Diaz, F. J. Desalination of brine by membrane distillation. *Desalination* **2001**, *137*, 267−273.

(12) Phattaranawik, J.; Jiraratananon, R.; Fane, A. G. Effects of net-type spacers on heat and mass transfer in direct contact membrane distillation and comparison with ultrafiltration studies. *J. Membr. Sci.* **2003**, *217*, 193−206.

(13) Calabro, V.; Jiao, B. L.; Drioli, E. Theoretical and experimental study on membrane distillation in the concentration of orange juice. *Ind. Eng. Chem. Res.* **1994**, *33*, 1803−1808.

(14) Van Gassel, T. J.; Schneider, K. An energy-efficient membrane distillation process. In *Membranes and Membrane Processes*; Drioli, E., Nagaki, M., Eds.; Plenum Press: New York, 1986; pp 343−348.

(15) Drioli, E.; Wu, Y.; Calabro, V. Membrane distillation in the treatment of aqueous solutions. *J. Membr. Sci.* **1987**, *33*, 277−284.

(16) Banat, F. A.; Simandl, J. Theoretical and experimental study in membrane distillation. *Desalination* **1994**, *95*, 39−52.

(17) Li, B.; Sirkar, K. K. Novel membrane and device for direct contact membrane distillation-based desalination process. *Ind. Eng. Chem. Res.* **2004**, *43*, 5300−5309.

(18) Li, B.; Sirkar, K. K. Novel membrane and device for vacuum membrane distillation-based desalination process. *J. Membr. Sci.* **2005**, *257*, 60−75.

(19) Wickramasinghe, S. R. J.; Semmens, M. J.; Cussler, E. L. Mass transfer in various hollow fiber geometries. *J. Membr. Sci.* **1992**, *69*, 235−250.

(20) Žukauskas, A. Heat transfer from tubes in crossflow. *Adv. Heat Transfer* **1987**, *18*, 87 − 159.

(21) Sieder, E. N.; Tate, C. E. Heat transfer and pressure drop of liquids in tubes. *Ind. Eng. Chem.* **1936**, *28*, 1429−1435.

(22) Guijt, C. M.; Meindersma, G. W.; Reith, T.; de Haan, A. B. Air gap membrane distillation 1. modeling and mass transport properties for hollow fiber membranes. *Sep. Purif. Technol.* **2005**, *43*, 233−244.

(23) Smith, J. M.; Van Ness, H. C.; Abbott, M. M. Vapor/Liquid Equilibrium: Introduction. *Introduction to Chemical Engineering Thermodynamics*, 6th ed. international ed.; McGraw-Hill Higher Education: New York, 2001; pp 328−367.

(24) Maron, M. J.; Lopez, R. J. *Numerical Analysis: A Practical Approach*; Wadsworth Publication: Belmont, CA, 1991, pp 210−214.

(25) Kreith, F.; Bohn, M. S. *Principles of Heat Transfer*, 6th ed.; Brooks/Cole: Pacific Grove, CA, 2001; Appendix 2, p A26.

(26) Mark, J. E. *Polymer Data Handbook*; Oxford University Press: New York, 1999.

Received for review July 28, 2006
Revised manuscript received January 2, 2007
Accepted January 9, 2007

IE0609968